Cell Reports
Physical Science

CellPress
OPEN ACCESS

Article

Selective phase transformation of layered double hydroxides into mixed metal oxides for catalytic CO oxidation

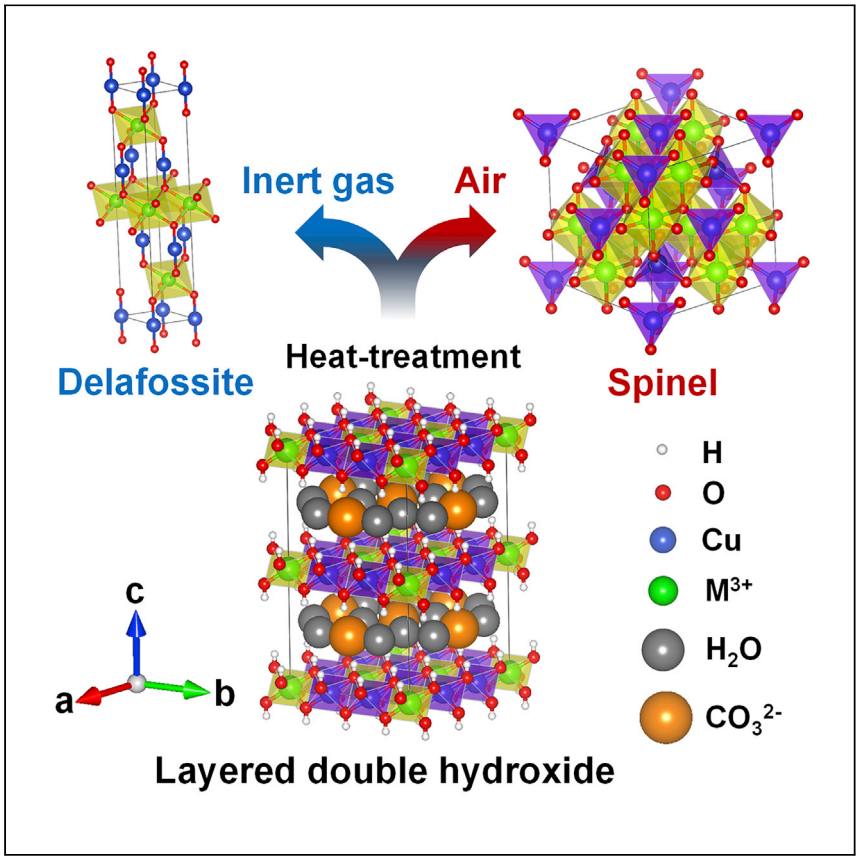

Synthesis of phase-pure materials is important for studying structure-property relationship. Jang et al. selectively prepared pure copper-based spinels and delafossites exploiting phase transformation of layered double hydroxides in different atmospheric conditions. The spinels exhibit higher CO oxidation activities and improved CO adsorption active sites than those of delafossites.

Wonsik Jang, Sinmyung Yoon, Jaejung Song, Jihun Kim, Kwangjin An, Seungho Cho

kjan@unist.ac.kr (K.A.)
scho@unist.ac.kr (S.C.)

Highlights

Preparation of copper-based layered double hydroxides (LDHs)

Selective phase transformation of LDHs into metal oxides

Phase dependence of catalytic carbon monoxide oxidation is studied

Jang et al., Cell Reports Physical Science 2, 100628
November 17, 2021
https://doi.org/10.1016/j.xcrp.2021.100628

Cell Reports
Physical Science

CellPress
OPEN ACCESS

Article

Selective phase transformation of layered double hydroxides into mixed metal oxides for catalytic CO oxidation

Wonsik Jang,[1,3] Sinmyung Yoon,[2,3] Jaejung Song,[1,3] Jihun Kim,[2] Kwangjin An,[2,*] and Seungho Cho[1,4,*]

SUMMARY

Phase transformation from layered double hydroxides (LDHs) into mixed metal oxides (MMOs) has been widely used in various catalytic applications owing to its numerous advantages over conventional synthesis methods. Herein we report the results of selective phase transformation of LDHs into spinels and delafossites for the preparation of phase-pure MMO catalysts. Pure cuprous delafossites and cupric spinels were selectively obtained through heat treatment of Cu-based LDHs followed by post-treatments. This enabled the study of the crystalline-phase-dependent CO oxidation activity of the MMO catalysts and their physicochemical properties. The spinel catalysts exhibited higher CO oxidation activities, in comparison with those of the delafossites, with greater redox properties and improved active sites for CO adsorption. Although the crystalline phases were derived from the same LDH precursors, the catalytic properties of the end product were greatly influenced by their crystal structures.

INTRODUCTION

Generally, different materials can be composed of the same elements and have the same compositions. Despite this similarity, they can exhibit distinctly different physicochemical properties depending on their crystal structures (phases).[1,2] Therefore, phase-selective synthesis is indispensable for developing materials with desired functional properties. Noteworthy examples of materials that consist of the same elements but have different crystal structures are spinels and delafossites. Both of these materials can have the same cation as one of their structural components. The spinel has a crystal structure with the general formula, $A_xB_{3-x}O_4$, which is isotypic with $MgAl_2O_4$.[3] As shown in Figure 1A, the divalent (A) and trivalent (B) cations occupy the tetrahedral and octahedral sites, respectively, in an oxygen array of a normal spinel (degree of inversion, $\gamma = 0$). Further, the cations A and B can swap their sites in a spinel, and their site preferences are affected primarily by their respective cation sizes and the ligand field stabilization energy.[4] An inverse spinel structure ($\gamma = 1$) is formed when all the A cations occupy the octahedral sites and half of the B cations occupy the tetrahedral sites. The inverse and mixed spinels ($0 < \gamma < 1$) exhibit functional properties that are different from those of the normal spinels.[5] Owing to their unique features including cationic inversion ability, spinels have been used in various fields, such as catalysis, magnetism, and energy conversion.[6–8]

The delafossite, another crystal structure with the general formula ABO_2, has garnered significant interest because of its unique electrical, magnetic, optical, and catalytic properties.[9–13] In particular, delafossite can have a wide range of

[1]Department of Materials Science and Engineering, Ulsan National Institute of Science and Technology (UNIST), Ulsan 44919, Republic of Korea

[2]Department of Energy and Chemical Engineering, Ulsan National Institute of Science and Technology (UNIST), Ulsan 44919, Republic of Korea

[3]These authors contributed equally

[4]Lead contact

*Correspondence: kjan@unist.ac.kr (K.A.), scho@unist.ac.kr (S.C.)

https://doi.org/10.1016/j.xcrp.2021.100628

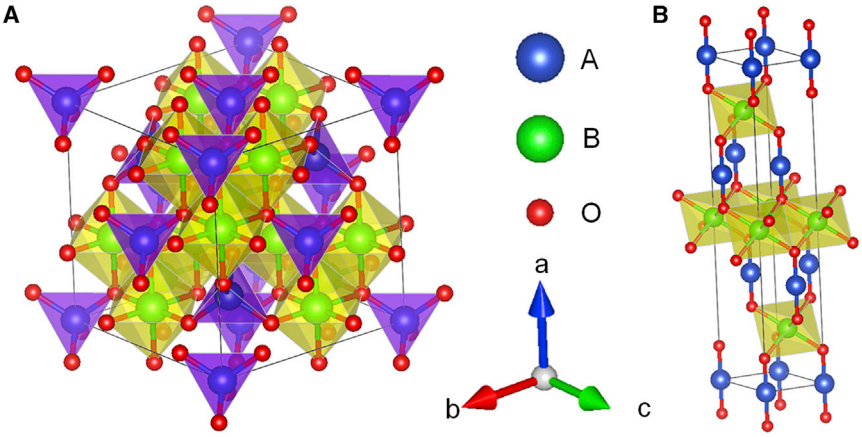

Figure 1. Illustrations of the Crystal structures
(A) AB_2O_4 Spinel structures.
(B) ABO_2 Delafossite structures.

conductivities, from insulating to semimetallic depending on its constituent elements. Figure 1B shows the generic structure of a delafossite crystal. The monovalent cations are linearly coordinated to two oxygen anions in the A-sites. The trivalent metal cations are located in the centers of the distorted edge-sharing BO_6 octahedrons (B-sites). An oxygen atom is located in a configuration of pseudo-tetrahedral coordination as B_3AO. Only four types of cations, that is, the cations of Cu, Ag, Pd, and Pt have been reportedly used as A-site cations in delafossite structures.[14,15] Among them, Cu is earth-abundant, and its delafossite form (i.e., cuprous delafossite) can exhibit p-type transparent conducting oxide (p-TCO) behaviors.[16] Thus, components made of cuprous delafossites are promising candidates for developing electrochemical devices that can perform CO_2 reduction, water splitting, gas sensing, and solar energy conversion.[17–21] Cu can possess monovalent as well as divalent chemical valence states; hence, it can be a constituent cation in both spinel and delafossite structures.

Layered double hydroxides (LDHs) have been widely used as the precursors for producing mixed metal oxides (MMOs).[22–26] LDHs, also known as hydrotalcite-like compounds, are a class of materials that have lamellar structures with positively charged host layers in which two or more types of metal cations are immobilized by the hydroxide anion arrays with uniform distribution.[27] In general, it is relatively difficult to precisely control the composition of the products in solution-based synthesis methods as compared to physical vapor deposition techniques. However, owing to their unique structures, we can tune the elemental constitution of LDHs while readily synthesizing them by the solution-based synthesis methods.[28,29] Therefore, MMOs that are derived from the LDHs have precisely controlled elemental compositions as well as certain additional advantages, such as controllable phase sizes and crystallographic orientations within the structures, which have tailored morphologies and particle sizes.[30,31] However, to date, only spinel-based MMOs transformed from LDHs have been reported, limiting their range of applications.

In this study we have achieved selective phase transformation of LDHs into delafossite- or spinel-based MMOs using rationally designed components that were generated during the heat treatment of the samples and their redox interactions. Initially, we successfully synthesized pure Cu-based LDHs containing Al, Cr, or Ga cations by a systematic parameter study including pH, aging temperature, and ionic size,

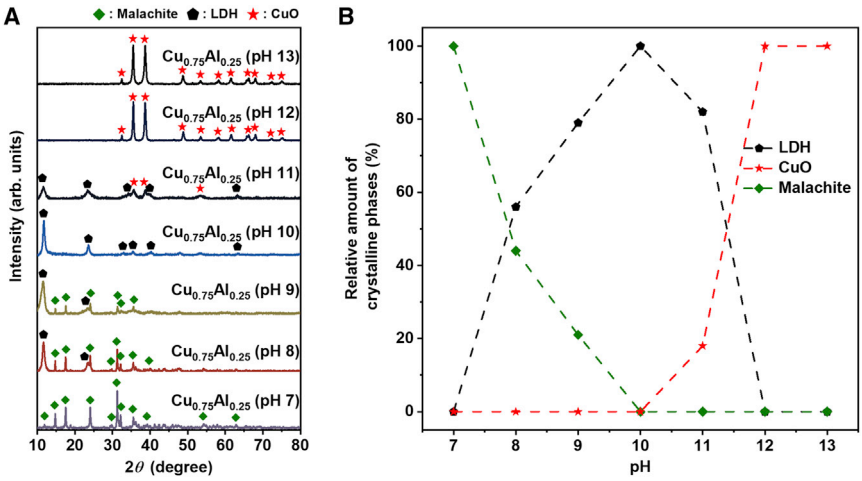

Figure 2. Influence of initial pH value on crystalline phases of final products

(A) X-ray diffraction patterns of CuAl-LDH samples prepared at different initial pH.

(B) Relative amounts of crystalline phases of the samples prepared at different initial pH.

although it is difficult to synthesize pure Cu-based LDHs owing to the formation of distorted Cu^{2+} octahedrons induced by the Jahn–Teller effect. The as-prepared pure Cu-based LDHs were transformed into delafossite- or spinel-based MMOs by controlling the atmospheric conditions under an inert atmosphere or in air during the heat treatment. Moreover, CuO and Cu_2O as components of MMOs can be selectively etched after acid treatment, leaving pure cuprous delafossites or cupric spinels as the end products. These selectively prepared pure-phase MMOs aided in a more precise study of the phase-dependent catalytic CO oxidation. CO oxidation ($2CO + O_2 \rightarrow 2CO_2$) has been designed to control emissions from combustion sources and it can be accomplished under mild reaction conditions with relatively rare side-reactions.[32–35] The CO oxidation reaction has been extensively studied as a model reaction due to industrial applications such as automotive exhaust gas treatment and CO removal in proton exchange membrane fuel cells. Basic studies on the catalysts in these model reactions can advance catalyst development for many catalytic processes. In addition, the principle underlying the difference in activity based on the structural differences of materials can be suggested through this model catalytic reaction. Thus, the structural effects of the selectively prepared phases (the Cu-based delafossites and spinels) on catalytic CO oxidation were further studied.

RESULTS AND DISCUSSION

Preparation and characterization of Cu-based layered double hydroxides

Preparation of pure LDHs as precursors are the prerequisites for selective phase transformation. Thus, the effects of various parameters including initial pH, aging temperature, and ionic size on the synthesis of LDHs were investigated. The parameter-based evaluation aided in the preparation of pure LDHs. Cu_3Al_1-LDHs were chosen as the model Cu-based LDHs because they are one of the most widely studied and used Cu-based LDHs. A coprecipitation method was used for the synthesis of CuAl-LDHs. The initial pH values of the synthesis solutions were varied to investigate the influence of pH on the formation of the precipitates. X-ray diffraction (XRD) patterns of the samples prepared with different initial pH are shown in Figure 2A. A qualitative inspection of the diffraction patterns suggests that initial pH values significantly affect the phase purity of the precipitates. The relative amounts of the

crystalline phases were estimated by integrating the areas of the reflections corresponding to each pattern and dividing the obtained values by the total area of all the reflections in the XRD patterns (Figure 2B).[36] CuAl-LDHs (ICDD 00-046-0099) were formed in the pH range of 8–11. In particular, CuAl-LDHs with no other crystalline phases were formed at pH 10. However, at a pH below 7, no LDH precipitation occurred since the solubility of the LDHs increases gradually under more acidic conditions.[37,38]

On the other hand, malachite was formed at a low pH regime. Since Cu^{2+} complexes with octahedral coordination are subject to the Jahn–Teller effect, the distorted Cu octahedrons can interact with the excess carbonate anions present in the reaction solution, thereby forming copper hydroxy complexes, such as malachite ($Cu_2(OH)_2CO_3$, ICDD 00-001-0959). The formation of malachite phases is competitive with the formation of LDHs because of the similar bond strengths of Cu^{2+}-CO_3^{2-} and Cu^{2+}-OH^-.[39,40] Owing to a relatively low concentration of OH^-, the formation of malachite can be dominant under low pH conditions following Equation (1). Likewise, an increase in the pH of the aqueous solution leads to the precipitation of LDHs predominantly following Equation (2). However, a highly basic condition (pH $\geq$ 11) adversely affects the stability of the LDHs.[41] Since the Jahn–Teller active Cu^{2+} prefers square-planar coordination geometries, the resulting copper hydroxy complexes are metastable and tend to transform into the more stable CuO (ICDD 01-089-5899) through dissolution and precipitation in an aqueous solution following Equation (3).[4,2] An excess of OH^- accelerates the dissolution rates of the copper hydroxy complexes.[42] Consequently, CuO formation was dominant at a pH above 11 in our experiment.

$$\begin{aligned} &6Cu^{2+}\,(aq) + 2Al^{3+}\,(aq) + 4CO_3^{2-}\,(aq) + 6OH^-\,(aq) \\ &\rightarrow 3Cu_2(OH)_2CO_3\,(s) + 2Al^{3+}\,(aq) + CO_3^{2-}\,(aq) \end{aligned} \quad (1)$$

$$\begin{aligned} &6Cu^{2+}\,(aq) + 2Al^{3+}\,(aq) + 4CO_3^{2-}\,(aq) + 16OH^-\,(aq) \\ &\rightarrow 6Cu(OH)_2\,(aq) + 2[Al(OH)_2]^+\,(aq) + 4CO_3^{2-}\,(aq) \\ &\rightarrow 8Cu_{0.75}Al_{0.25}(OH)_2[CO_3]_{0.125}\cdot mH_2O(s) + 3CO_3^{2-}\,(aq) \end{aligned} \quad (2)$$

$$\begin{aligned} &6Cu^{2+}\,(aq) + 2Al^{3+}\,(aq) + 4CO_3^{2-}\,(aq) + 24OH^-\,(aq) \\ &\rightarrow 6[Cu(OH)_4]^{2-}\,(aq) + 2Al^{3+}\,(aq) + 4CO_3^{2-}\,(aq) \\ &\rightarrow 6CuO\,(s) + 2Al^{3+}\,(aq) + 4CO_3^{2-}\,(aq) + 12OH^-\,(aq) + 6H_2O\,(l) \end{aligned} \quad (3)$$

Pure LDHs were formed at an initial pH of 10 (0.12 M CO_3^{2-}). However, the reaction solutions contained various anions including OH^-, NO_3^-, and CO_3^{2-}, which can interact with the Jahn–Teller active Cu^{2+} octahedrons. Therefore, the concentrations of such anions also have a strong influence on the formation of the LDHs. Figure S1 shows the XRD patterns of the precipitates prepared with different concentrations of CO_3^{2-}. The formation of malachite was dependent on the concentration of CO_3^{2-}. Thus, as the initial concentration of CO_3^{2-} increased to 0.8 M, a significant amount of malachite was formed even at the initial pH of 10 (Figure S1A). On the other hand, when the concentration of CO_3^{2-} decreased to 0.06 M, CuAl-LDHs were formed primarily at an initial pH of 9 (Figure S1B). Further decreasing the concentration of CO_3^{2-} to 0.03 M under the same initial pH condition (pH = 9) resulted in the formation of copper hydroxy nitrates $Cu_2(OH)_3NO_3$ (ICDD 00-015-0014) along with small amounts of LDHs (Figure S1C). However, in the absence of CO_3^{2-} (and at the same initial pH of 9), a nitrate-rich condition persisted, which led to the formation of copper hydroxy nitrate predominantly (Figure S1D).Reaction temperatures also

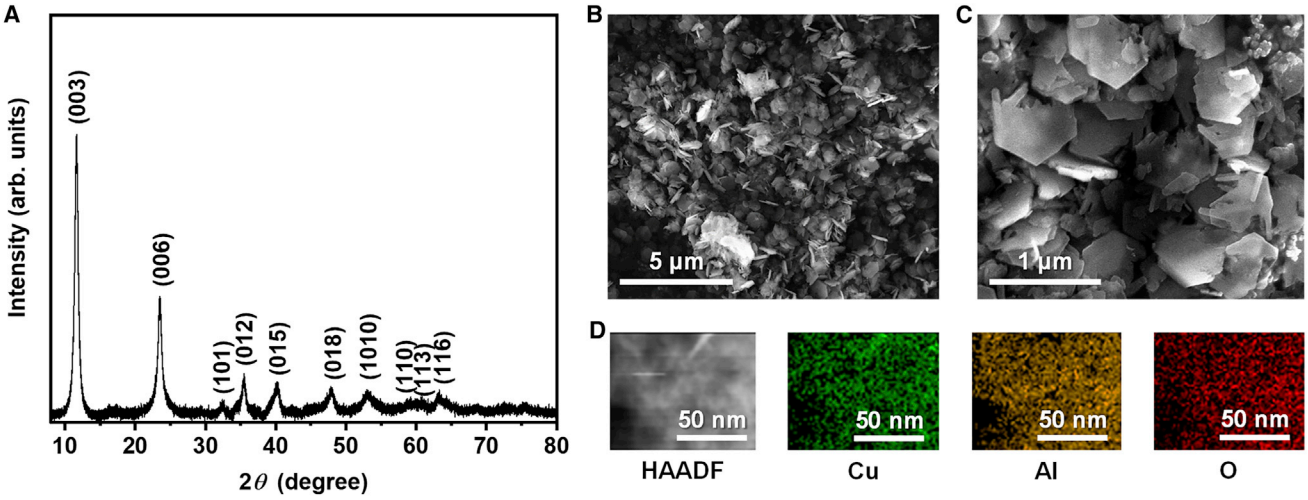

Figure 3. Characterization of CuAl-LDHs

(A) XRD pattern of CuAl-LDHs.

(B and C) SEM images of CuAl-LDHs.

(D) HAADF image and corresponding EDS elemental maps of CuAl-LDHs.

influence the formation and growth of various crystal structures, such as LDHs or oxide derivatives.[43] Separate nucleation and aging approaches have been widely used for the synthesis of LDHs providing better crystallinities, higher aspect ratios, and narrow crystal size distribution.[44] To investigate the influence of aging temperature on the formation and growth of LDHs, the reaction solutions were aged under various temperatures ranging from 30°C to 200°C after coprecipitation at a constant pH of 10. Subsequently, XRD and quantitative analysis of the final products were conducted (Figure S2). At 30°C, pure CuAl-LDHs were formed. A higher aging temperature (above 30°C) resulted in a slightly higher crystallinity with narrow full width at half maximum (FWHM) in the XRD peaks. However, the formation of an additional phase—CuO—was also detected by XRD. Generally, at high temperatures, most of the divalent metal hydroxides or hydroxy salts undergo thermal decomposition in an aqueous solution.[45] The metastable Cu hydroxy complexes that are derived from the Jahn–Teller effect decompose even at a lower temperature as compared to the other metal hydroxides, which are composed of stable brucite structures.[46] As a result, CuO and CuAl-LDHs were formed together in the temperature range of 45–90°C. Further, the relative amounts of CuO increased with the increasing aging temperatures. On the contrary, the relative amounts of CuAl-LDHs decreased as the aging temperatures were increased. At 150°C, the formation of CuO was dominant. As aging temperatures were further increased above 200°C, AlOOH (ICDD 01-072-0359) was formed together with CuO.

The XRD patterns, scanning electron microscopy (SEM) images, and energy dispersive spectroscopy (EDS) profiles of the CuAl-LDHs prepared at 30°C and initial pH of 10 are shown in Figure 3. In the XRD pattern, the diffraction peaks with 2θ angles of 11.7°, 23.6°, 32.8°, 35.6°, 40.4°, 48.0°, 53.3°, 58.9°, and 60.7° correspond to (003), (006), (101), (012), (015), (018), (1010), (110), and (113) reflections, respectively, for CuAl-LDHs (Figure 3A). Homogeneous nanoparticles are visible in the SEM image at low magnification (Figure 3B). At high magnification, two-dimensional hexagonal nanoplatelets, which are a typical LDH morphology, are observed (Figure 3C). A combination of high-angle annular dark field (HAADF) imaging and EDS elemental mapping of CuAl-LDHs (Figure 3D) shows that Cu, Al, and O are highly dispersed

in the LDH nanostructures. In addition, the observed atomic ratios are highly consistent with those in the reaction solution prior to the reaction (Figure S3).

We further investigated the feasibility of applying the optimized synthetic conditions to other elements and attempted to identify the particular conditions that should be met for incorporating other elements into the LDH structure. The process of formation of a crystal structure is strongly affected by the size of the constituent cations and anions. Following Pauling's first rule, a metal hydroxide octahedron remains stable unless the radii of the cations is less than 55 pm, assuming that the ionic radius of OH^- with coordination number 3 is 133 pm.[47] As the radii of cations increase beyond 98 pm, the cations gradually start preferring the higher coordination geometries over the octahedral one. Cu-based LDHs consisting of Cu^{2+} and other cations including Al^{3+}, Cr^{3+}, Ga^{3+}, Zn^{2+}, Co^{2+}, Ni^{2+}, and Mg^{2+}, which satisfy the Pauling's rule, were formed without other crystalline phases under the optimized synthetic condition (Figure S4). However, in the case of Sr, Y, La, and Bi, which have relatively large ionic radii, other crystalline phases were formed under the synthetic condition (Figure S5). A structure field map containing the ionic radii of various groups of elements is provided in Figure S6. The metal cations (possessing suitable ionic sizes), which can be inserted in the hydroxide octahedrons following Pauling's first rule, are located in the shaded region. The cations marked in green or red indicate those ions whose addition resulted in a successful or failed LDH synthesis, respectively. Furthermore, the cations highlighted in blue were reported in literature (Table S1). It is noteworthy that most of the cations that are mentioned in the structure map obey Pauling's first rule (Figure S6).

Selective phase transformation of layered double hydroxides into spinels and delafossites

It is well known that the thermal treatment of LDHs at high temperatures leads to their phase transformation into spinel-based composites owing to the presence of both divalent and trivalent metal cations in the LDH structures. However, in the case of Cu-based LDHs, the selective phase transformation into delafossites and spinels is feasible for the following reasons. Both monovalent and divalent Cu cations are stable; thus, divalent copper oxides can be decomposed into monovalent copper oxides under inert or reducing conditions at high temperatures.[48,49] The selective phase transformation mechanism of CuAl-LDHs into spinels or delafossites during heat treatment in air or under inert conditions was evaluated using simultaneous differential scanning calorimetry and thermogravimetric analysis (SDT) and *ex situ* XRD analysis in the temperature range of 25°C–1000°C (Figure 4). The XRD patterns were obtained at intervals of 50°C after the sample was held at the reaction temperature for 1 h before the measurement. As shown in Figure 4A, the TG curve of CuAl-LDHs in air exhibited three major weight losses. The first sharp weight loss region at approximately 150°C corresponds to the evaporation of water from the interlayer of LDH structures (Equation (4)).[50] The removal of water from the interlayer region can also be identified from the XRD patterns. At 150°C, the d_{003}-spacing of CuAl-LDHs decreased owing to the removal of water from the interlayer as shown in Figure 4C. In the second broad weight loss region ranging from 150°C to 400°C, the weight loss due to the decomposition of carbonate anions in the interlayer regions and that due to the dehydroxylation of the host layers overlapped.[51] No characteristic XRD patterns of the LDHs were observed above 200°C, indicating the decomposition of the LDH structures. After the decomposition of the LDH structure above 400°C, the resultant products formed crystalline CuO as shown in Figure 4C [Equation (5)]. The Al species existed in the amorphous phase in the products without forming crystalline phases such as Al_2O_3 owing to the high dispersion caused by the LDH

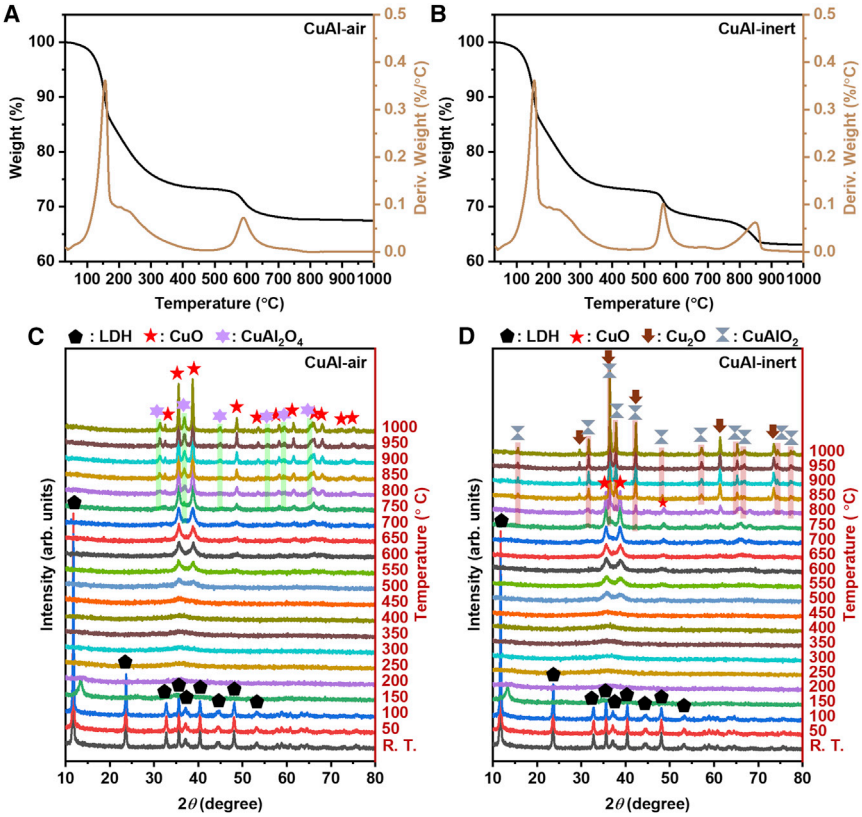

Figure 4. SDT and *ex situ* XRD patterns of CuAl-LDHs in air or under inert conditions

(A) SDT of CuAl-LDHs in air.

(B) *ex situ* XRD patterns of CuAl-LDHs in air.

(C) SDT of CuAl-LDHs under inert condition.

(D) *ex situ* XRD patterns of CuAl-LDHs under inert condition.

precursor. When the CuAl-LDHs were treated at higher temperatures over 400°C, the crystallinity of the Al-doped CuO increased with a narrower FWHM as the treatment temperature increased. The third weight loss was due to the aggregation of the Al-doped CuO, as the Tamman temperature of CuO is reported to be over 550°C.[52] When the crystallite of Al-doped CuO sufficiently grew, the phase separation of Al-doped CuO into cupric spinel and CuO occurred following Equation (6). The XRD patterns of the $CuAl_2O_4$ spinel structure became observable when the CuAl-LDHs underwent heat treatment at 750°C and the crystallinity increased with even higher temperatures as shown in Figure 4C.

$$Cu_{0.75}Al_{0.25}(OH)_2[CO_3]_{0.125}\cdot mH_2O\ (s) \rightarrow Cu_{0.75}Al_{0.25}(OH)_2[CO_3]_{0.125}(s) + mH_2O\ (g) \quad (4)$$

$$8Cu_{0.75}Al_{0.25}(OH)_2[CO_3]_{0.125}(s) \rightarrow 8Cu_{0.75}Al_{0.25}O_{1.125}(s) + CO_2\ (g) + 8H_2O\ (g) \quad (5)$$

$$8Cu_{0.75}Al_{0.25}O_{1.125}(s) \rightarrow CuAl_2O_4\ (s) + 5CuO\ (s) \quad (6)$$

The phase transformation under inert conditions was also investigated as shown in Figures 4B and 4D. The TG curve of the CuAl-LDHs under inert conditions demonstrated a similar tendency to that of the TG curve treated in air except for an additional weight loss in the range of 750°C–850°C. The additional weight loss corresponds to the deoxygenation process due to the decomposition of divalent

copper oxides into monovalent copper oxides under inert conditions following Equation (7). In this stage, $CuAl_2O_4$ spinels were also decomposed into $CuAlO_2$ delafossites. Furthermore, when CuO co-exists in the cupric spinel composites, the decomposition rate of the spinel is accelerated under inert conditions, because Equation (8) is energetically preferred to Equation (9) under inert conditions.[49,53] The resultant products from thermal treatment of Cu-based LDHs are complex MMOs, which contain an excess of copper oxides (CuO and Cu_2O) as well as spinels. Thus, the excess amount of CuO enables the fast decomposition of spinels into delafossites under inert conditions. Consequently, the process of formation and decomposition of spinels can occur simultaneously under inert conditions, and hence, selective phase transformation from Cu-based LDHs into spinels and delafossites can be achieved by simply adjusting the atmospheric conditions. The XRD patterns of the $CuAlO_2$ delafossite structures were observable from temperatures of 750°C onward, and the crystallinity sufficiently increased at temperatures over 850°C to be distinguishable under inert conditions, as shown in Figures 4B and 4D. Therefore, the temperature required for the selective preparation of spinels and delafossites should be at least 850°C or higher.

$$2CuO\ (s) \rightarrow Cu_2O\ (s) + \frac{1}{2}O_2(g) \quad (7)$$

$$CuO\ (s) + CuAl_2O_4\ (s) \rightarrow 2CuAlO_2\ (s) + \frac{1}{2}O_2\ (g) \quad (8)$$

$$2CuAl_2O_4\ (s) \rightarrow 2CuAlO_2\ (s) + Al_2O_3\ (s) + \frac{1}{2}O_2\ (g) \quad (9)$$

Among the seven types of the as-prepared Cu-based LDHs, three types of bimetallic LDHs containing Al^{3+}, Cr^{3+}, or Ga^{3+} were chosen and heat-treated under an inert atmosphere or in air for selective phase transformation into delafossite- or spinel-based composites. CuAl-, CuCr-, and CuGa-LDHs were heat-treated at 850°C, 700°C, and 1000°C, respectively, under air or inert atmosphere. Consequently, three types of Cu-based LDHs were selectively phase transformed into crystalline spinel composites and delafossite composites under air and inert atmosphere, respectively, as shown in Figure S7. Subsequently, an acid treatment was performed to dissolve the other phases, such as copper oxides (CuO and Cu_2O). Based on the chemical composition of Cu and Al in the MMOs determined using inductively coupled plasma optical emission spectroscopy (ICP-OES) before and after etching (Table S2), it is evident that the acid treatment selectively removed the copper oxides from the spinel and delafossite composites. As a result, we successfully prepared: (1) pure cuprous delafossites, including $CuAlO_2$ (ICDD 00-035-1401), $CuCrO_2$ (ICDD 00-074-0983), and $CuGaO_2$ (ICDD 00-041-0255) by heat treating the LDHs under inert conditions (Figures 5A–5C); and (2) cupric spinels, including $CuAl_2O_4$ (ICDD 01-076-2295), $CuCr_2O_4$ (ICDD 01-087-0432), and $CuGa_2O_4$ (ICDD 01-078-0172), by heat treating the LDHs in air (Figures 5D–5F). The microstructure and morphology of the fabricated pure cuprous delafossites and cupric spinels are depicted in Figure S8.

X-ray photoelectron spectroscopy (XPS) was performed to investigate the chemical valence states of the delafossite and spinel structures. The Cu 2p core-level spectra of the delafossites and spinels are shown in Figure 6. The intense Cu $2p_{1/2}$ and $2p_{3/2}$ peaks at 952 and 932 eV ($\pm$0.2 eV), respectively (Figures 6A, 6B, and 6C), indicate that the Cu has an oxidation state of +1 in the delafossite structures. On the other hand, the major oxidation state of Cu is +2 in the spinel structures (Figures 6D,

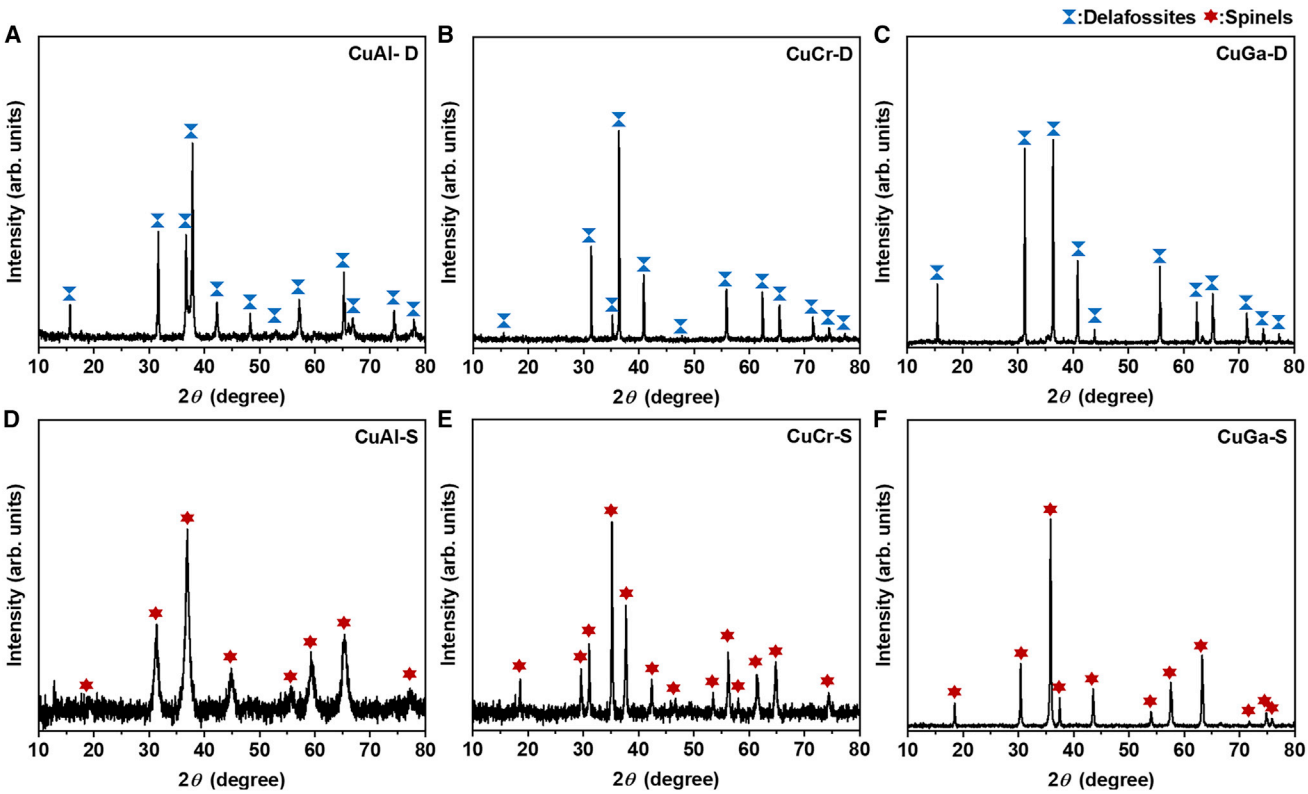

Figure 5. XRD patterns of Cu-based delafossites and spinels

(A) CuAl-delafossites.
(B) CuCr-delafossites.
(C) CuGa-delafossites.
(D) CuAl-spinels.
(E) CuCr-spinels.
(F) CuGa-spinels.

6E, and 6F). The Cu $2p_{1/2}$ and $2p_{3/2}$ peaks at 954.4 and 934.6 eV ($\pm$0.1 eV), respectively, are assigned to Cu^{2+}; further, the strong satellite peaks observed at approximately 961.6, 943.3, and 940.8 eV indicate the presence of an unfilled $3d^9$ shell in the Cu^{2+} species.[54–56] Therefore, the XPS results reveal that for all Cu-based oxides, the monovalent state is dominant in the delafossite structures and the divalent state is dominant in the spinel structures. On the contrary, all B-site atoms, including Al, Cr, and Ga, have trivalent states in the delafossites and spinels (Figure S9).[57–59] Thus, on the basis of the combined XRD and XPS analysis, it is verified that the selective preparation of pure delafossites and spinels employing phase transformation of LDHs was achieved.

Relationship between crystal structure and catalytic activity for CO oxidation

Catalytic CO oxidation was performed as a model reaction to investigate the structural effect of the Cu-based delafossites and spinels. Copper oxide is well known to be active in CO oxidation by itself or in combination with a support oxide, such as CeO_2.[60] The oxidation state of copper oxide is a crucial factor in catalytic activity owing to its distinct redox behavior.[61,62] Figure 7A shows the catalytic activities of the Cu-based delafossites and spinels in CO oxidation. Cu-based spinel structures exhibit higher activities than the corresponding delafossite structures. In particular, based on the temperatures at which the CO conversion of the catalyst reaches 50%

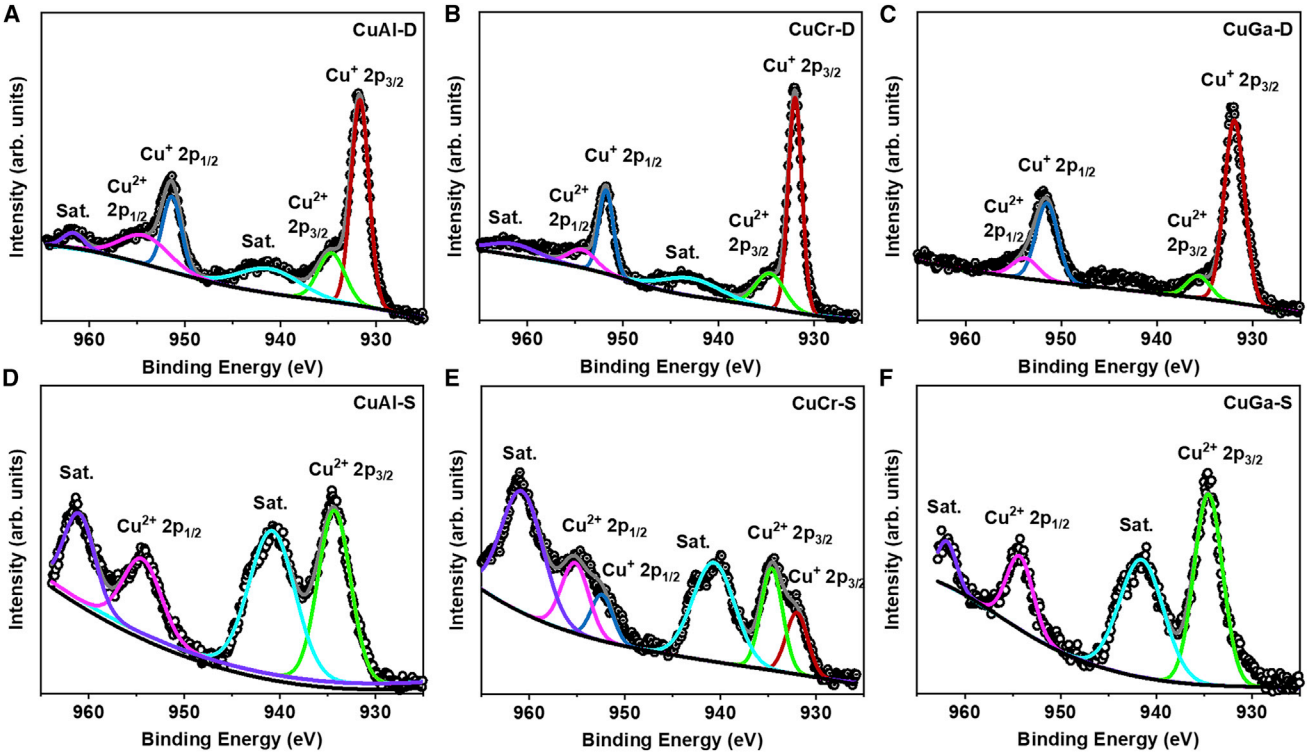

Figure 6. XPS profiles (Cu 2p) of Cu-based delafossites and spinels

(A) CuAl- delafossites.
(B) CuCr- delafossites.
(C) CuGa-delafossites.
(D) CuAl-spinels.
(E) CuCr-spinels.
(F) CuGa-spinels.

(T_{50}), the maximum activity gap is observed in the CuGa-based catalysts (T_{50} = 235°C and 450°C for spinel and delafossite, respectively). The T_{50} values of the catalysts are shown with error bars in Figure 7B. To investigate the effect of B-site atoms (Al, Cr, and Ga) on the catalytic properties of the cuprous delafossites and cupric spinels, Cu-free defective spinel-type structures[63] with octahedral coordinated cations were synthesized, including Al_2O_3, Cr_2O_3, and Ga_2O_3. For a precise comparison, all Cu-free samples and their corresponding Cu-based spinels were prepared under equivalent conditions. As shown in Figure S10, each Cu-free hydroxy complex precursor was synthesized without any impurities under conditions same as that for the Cu-based LDH synthesis (Figures S10A–S10C), followed by calcination at the same temperatures for the formation of the corresponding Cu-based spinel structures (Figures S10D–S10F). We observed negligible catalytic activities in Al_2O_3 and Ga_2O_3 and less than 20% CO conversion in Cr_2O_3 up to 450°C (Figure S11). This indicates that Al, Cr, and Ga are nonredox entities having negligible effect on the catalytic activities. Further, the Cu species in the delafossites and spinels are the active sites determining the catalytic performances (Figure 6).[64,65]

The redox properties have a decisive influence on the catalytic CO oxidation of Cu-based catalysts operating under a redox-type catalytic mechanism, wherein the reactant CO and O_2 act as the reductant and oxidant, respectively.[66–68] Therefore, the redox behaviors of the Cu-based delafossites and spinels were investigated

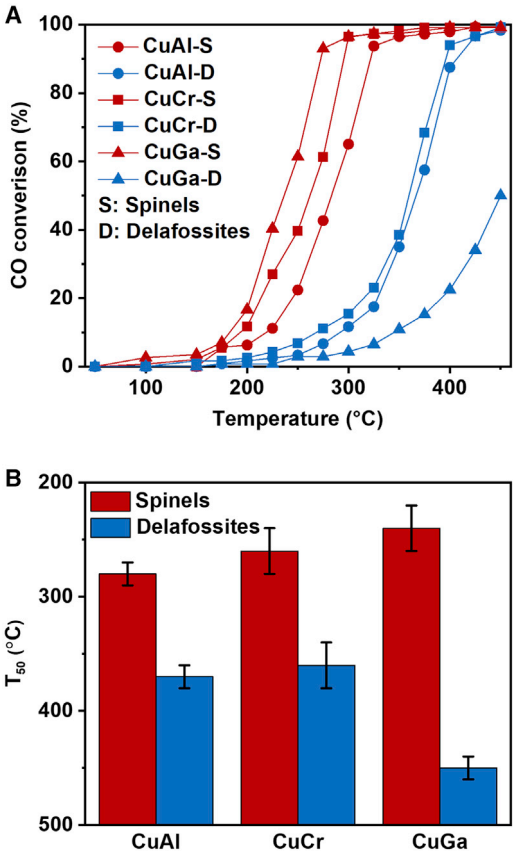

Figure 7. CO oxidation results of the Cu-based delafossites and spinels

(A) CO conversion in the temperature range of 50–450°C.

(B) Temperatures at which the CO conversion of the catalyst reached 50%. Error bars were determined by repeating the measurements thrice.

through temperature-programmed reduction (TPR) with H_2 flow (H_2-TPR) by measuring their H_2 consumption (Figure 8) and *in situ* XRD analysis under H_2 atmosphere (Figures S12–S14). The reduction peaks of all the spinel oxides appeared at much lower temperatures than the delafossite peaks (Figure 8). The Cu-based spinels show two characteristic peaks: α and β. The first peak (α) indicates a reduction from Cu^{2+} to Cu^{+} in the temperature range of 200°C–300°C.[69] The reduction temperatures assigned to the α peaks between 200°C and 300°C are consistent with the reaction temperatures of the spinels (Figure 7A). The enhanced catalytic activities of the spinels in CO oxidation originate from the additional reduction steps. Qi et al. demonstrated that the presence of an additional reduction step of Cu^{2+} to Cu^{1+} stimulates an easier reduction of CuO as compared to Cu_2O.[70] The second peak (β) originates from the reduction of Cu from Cu^{+} to Cu^{0}. On the other hand, since the oxidation states of Cu in the Cu-based delafossites are monovalent, they show only a single characteristic peak, δ, which indicates a reduction from Cu^{+} to Cu^{0}. According to the *in situ* XRD results (Figures S12–S14), the cuprous delafossites and cupric spinels decompose into metallic Cu (ICDD 00-001-1241) while retaining their Cu-deficient characteristics under the H_2 conditions. The additional peak (δ) is also observed in the H_2-TPR result of the CuCr-spinels. Unlike the other Cu-based spinels (Al and Ga), CuCr-spinels undergo phase transformation to yield CuCr-delafossites under reducing conditions (Figure S13), resulting in the additional δ peak. Interestingly, the reduction temperature corresponding to the δ peak in

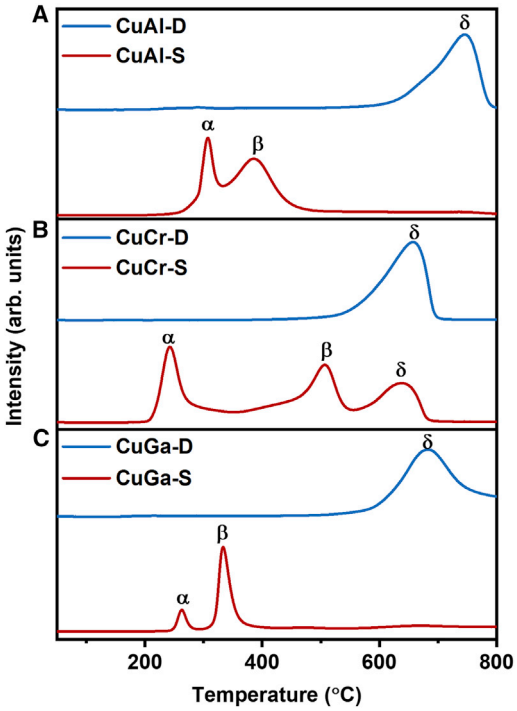

Figure 8. H_2-TPR spectra of Cu-based delafossites and spinels

(A) CuAl- delafossites and spinels.

(B) CuCr- delafossites and spinels.

(C) CuGa-delafossites and spinels.

the delafossites is significantly higher than that of the β peak in the spinels. This higher reduction temperature implies that spinels have greater redox properties than those of delafossites.[71] The differing redox behaviors are also confirmed by the *in situ* XRD results, which exhibit a higher reduction temperature corresponding to Cu^0 in the delafossite structures (Figures S12–S14). The reduction from Cu^{2+} to Cu^0 is thermodynamically more favorable than that from Cu^+ to Cu^0.[72] In addition, the delafossite structures exhibit higher stability than the spinel structures under reducing conditions.[73] Therefore, spinels have much higher redox properties than delafossites, and as a result, show enhanced catalytic CO oxidation activities.

Further probe behavior differences during adsorption using probe molecule IR spectroscopy demonstrate the reaction pathway for the catalytic reactions. The CO stretching characteristics distinguish the adsorption site for the CO oxidation reaction by identifying structure-dependent active sites.[74,75] In addition to the previous CO conversion and redox properties, CO adsorption behavior was compared in spinel and delafossite structures through diffuse reflectance infrared Fourier transform spectroscopy (DRIFTS) analysis. DRIFTS was conducted by varying the sequential gas flow conditions of CO adsorption, He purging, and CO desorption by increasing the temperature under an O_2 atmosphere (Figure S15). In the case of cupric spinels (CuGa-spinel and CuAl-spinel), the CO adsorption peak at 2130–2140 cm^{-1} remained after He purging, indicating the CO chemical adsorption onto the spinel structure. The resulting CO vibration exhibited a peak shift in the spinel composites,[76] and this significant adsorption peak diminished after O_2 treatment. However, CuCr-spinel exhibits a strong absorption of the IR beam, making it difficult to analyze DRIFTS. Nevertheless, no significant adsorption peak remained after He purging in the cuprous delafossite structures. These results suggest that a larger number of CO adsorption sites are secured in the spinel structure than those in the delafossite structure, suggesting a high CO oxidation activity in the spinel structure.

In addition to the redox properties and active sites for CO adsorption, the size-dependent catalytic CO oxidation activities have been often reported in Cu-based MMO catalysts.[77–79] Therefore, the particle sizes, crystallite sizes, and surface areas of the catalysts were determined, as presented in Table S3. The particle sizes of the catalysts were calculated using "Image J software" from Figure S8.[79] The SEM images of cuprous delafossites and cupric spinels (Figure S8) exhibited similar morphologies and particle sizes for each cation combination owing to the topological phase transformation of the LDHs. Brunauer–Emmett–Teller (BET) surface areas of the catalysts were measured by performing N_2 adsorption experiments (Figure S16). The results show that the BET surface area of each type of spinel is slightly higher than that of the corresponding delafossite. In addition, the average crystallite sizes were calculated from Figure 4 using Scherrer's equation with a constant shape factor (K) of 0.9. The average crystallite size of each type of spinel is smaller than its delafossite counterpart. This observation is consistent with the corresponding BET results. Generally, delafossite crystals grow larger than spinels under identical growth conditions,[36] as they require higher formation energy as compared to spinels.[48] However, the size differences between the corresponding delafossites and spinels are insignificant and the surface areas of both structures are not large (less than 100 m^2g^{-1}) to produce significant change in their catalytic activities. From these results, we can infer that the variations in the catalytic activities emerged mainly from the hugely different redox properties of the delafossite and spinel structures, as evident from the H_2-TPR spectra shown in Figure 8.

In summary, pure Cu-based LDHs were synthesized and examined by a systematic parameter study. Subsequently, selective phase transformations into a set of cuprous delafossites and cupric spinels were achieved by heat treating the fabricated LDHs under different atmospheric conditions. This phase transformation step was followed by a selective etching of the impurities. The purity of the synthesized delafossites and spinels was verified by a combined XRD and XPS analysis. The evaluation of the structure–catalytic activity relation revealed that spinels exhibit higher CO oxidation activities as compared to the delafossites regardless of the nature of the B-site atoms. The redox properties, catalytic active sites, and sizes of the catalysts, which have a significant influence on the catalytic activities, were thoroughly investigated by H_2-TPR, CO-DRIFTS, and calculating the particle sizes, crystallite sizes, and BET surface areas. Consequently, the greater redox properties, and more active sites for CO adsorption of cupric spinel catalysts in comparison with those of the cuprous delafossite catalysts resulted in greater CO oxidation activities. The phase-selective synthesis process highlights the dependency of structures on their respective physicochemical properties by minimizing the extrinsic variabilities. Furthermore, such phase-selective transformations of the precursors may provide a new avenue for fabricating advanced materials imbued with tunable functional properties for various applications.

EXPERIMENTAL PROCEDURES

Resource availability

Lead contact

Further information and requests for resources and reagents should be directed to and will be fulfilled by the lead contact, Seungho Cho (scho@unist.ac.kr).

Materials availability

All of the materials generated in this study are available from the lead contact without restriction.

Data and code availability

The authors declare that data supporting the results of this study are available in the main text and supplemental information. Further information and requests for additional data should be directed to the Lead Contact.

Synthesis of Cu-based LDHs

$Cu(NO_3)_2 \cdot 3H_2O$, $Al(NO_3)_3 \cdot 9H_2O$, $Cr(NO_3)_3 \cdot 9H_2O$, $Ga(NO_3)_3 \cdot xH_2O$, $Zn(NO_3)_2 \cdot 6H_2O$, $Mg(NO_3)_2 \cdot 6H_2O$, $Co(NO_3)_2 \cdot 6H_2O$, $Ni(NO_3)_2 \cdot 6H_2O$, Na_2CO_3, and NaOH solution (2 N) (Sigma-Aldrich) along with nitric acid (65%) and ammonia solution (28∼30%) (Samchun Chemicals) were used in the form delivered by the manufacturer without any further purification. Deionized (DI) water, for preparing the metal precursor solutions, was obtained by triple distillation and purification using a Millipore filtration system.

The synthesis of the CuAl-LDHs that was investigated in this study was performed using the co-precipitation method at a constant pH. In detail, 18 mmol $Cu(NO_3)_2 \cdot 3H_2O$, 12 mmol Na_2CO_3, and 6 mmol $Al(NO_3)_3 \cdot 9H_2O$ were dissolved in the DI water (100 mL) while stirring the solution at 500 rpm at 22°C. NaOH solution was added dropwise to the mixture until the pH value reaches 10 ($\pm$0.1). The mixture was aged in an oven at 30°C for 24 h. After the reaction, the resulting suspension was separated using a centrifuge at 5000 rpm for 3 min and subsequently washed thrice with DI water and ethanol. The separated slurry was dried in an oven at 60°C for 12 h. In case of synthesis of CuCr-LDHs or CuGa-LDHs, $Al(NO_3)_3 \cdot 9H_2O$ were replaced by $Cr(NO_3)_3 \cdot 9H_2O$ or $Ga(NO_3)_3 \cdot xH_2O$ in the equivalent conditions.

Synthesis of cupric spinel and cuprous delafossite

2 g of Cu-based LDHs were heated using a tube furnace (SH scientific SH-FU-50TH) for 1 h at a heating rate of 10°C min^{-1} to the desired reaction temperatures under an inert atmosphere for producing delafossites or in the air for developing spinels followed by slowly cooling the samples to room temperature. To maintain an inert atmosphere, the tube furnace was continuously filled with Ar gas at a flow rate of 100 mL·min^{-1} throughout the reaction. A mass flow controller (ICDS FM-30VP) was used for precisely controlling the Ar flow rate. For the selective dissolution of the copper oxides, the MMOs were added to and stirred for 30 min in an acidic solution prepared by mixing nitric acid (7 mL) and DI water (3 mL). This solution was filtered to obtain the resulting powder, which was dried at 60°C for 12 h.

Characterization

XRD measurements were performed using a Bruker AXS D8 ADVANCE X-ray diffractometer, which is equipped with Cu Kα radiation (1.5406 Å). The data were collected in the angular range $10^\circ \leq 2\theta \leq 80^\circ$ with an irradiation time and a step increment of 0.25 s and 0.02°, respectively. The SEM images of the samples were taken with a Hitachi S-4800 system. Further, the TEM images and EDS data were obtained using an FEI Tecnai G2 F20 X-Twin system. XPS profiles of the MMOs were recorded with a Thermo-Fisher K-alpha system, which has a monochromatic Al Kα (8.339 Å) X-ray source. The spectra of binding energies were calibrated with the C 1 s peak at 284.8 eV as the internal standard, and the multiple peaks were fitted and deconvoluted via Gaussian fitting. Thermal analysis was investigated at a heating rate of 10°C min^{-1} from room temperature to 1000°C using SDT (TA Q600). Under inert conditions, thermal analysis was conducted under N_2 flow at a flow rate of 100 mL·min^{-1}. H_2-TPR was conducted using a BELCAT II catalyst analyzer. The catalyst (50 mg) was pretreated at 100°C under Ar flow (30 mL min^{-1}) for 1 h. After cooling, the temperature was increased under 5% H_2 and 95% Ar flow (30 mL min^{-1}) to 800°C at a heating rate of 10°C min^{-1}. H_2 consumption was monitored by a thermal conductivity detector (TCD).

Catalyst testing

The catalytic CO oxidation was carried out in a quartz fixed-bed reactor with 50 mg of catalyst mixed with 100 mg of quartz powder (to avoid mass and heat transfer limitations). The temperature was measured by a thermocouple located close to the reactor. Prior to the measurements, the catalyst was pretreated at 100°C under Ar flow for 1 h. CO oxidation was performed with a feed stream consisting of 2% CO and 2% O_2, balanced with Ar. The total flow rate was 50 mL min^{-1} and the heating rate was 5°C min^{-1}. The catalyst was maintained at each temperature for 10 min in a continuous feed flow to reach a steady state before the actual analysis. The products were detected by a GC (YL-6500) system equipped with a Carboxen 1000 column (Supelco) and a TCD.

SUPPLEMENTAL INFORMATION

Supplemental information can be found online at https://doi.org/10.1016/j.xcrp.2021.100628.

ACKNOWLEDGMENTS

The study was financially supported by the 2021 Research Fund (1.210035.01) of UNIST (Ulsan National Institute of Science & Technology), the National Research Foundation of Korea (NRF) through a grant funded by the Korean government (MSIT: Ministry of Science and ICT; Grant Nos. NRF-2018R1C1B6002342, NRF-2019M1A2A2065612, and NRF-2020R1A5A1019631), and the Technology Innovation Program by the Ministry of Trade, Industry & Energy (MOTIE, 20012971 and 20015619).

AUTHOR CONTRIBUTIONS

W.J. and S.C. conceived the concept of selective phase transformation of LDHs into delafossites and spinels. S.C. and K.A. designed and supervised the research. W.J. and J.S. synthesized and characterized Cu-based LDHs, cuprous delafossites, and cupric spinels. S.Y. and J.K. measured the CO oxidation properties. W.J., S.Y., J.S., K.A., and S.C. co-wrote the manuscript. All authors read and commented on the manuscript.

DECLARATION OF INTERESTS

The authors declare no competing financial interests.

Received: April 30, 2021
Revised: September 7, 2021
Accepted: October 7, 2021
Published: November 3, 2021

REFERENCES

1. Jubb, A.M., and Allen, H.C. (2010). Vibrational spectroscopic characterization of hematite, maghemite, and magnetite thin films produced by vapor deposition. ACS Appl. Mater. Interfaces *2*, 2804–2812.

2. Teja, A.S., and Koh, P.-Y. (2009). Synthesis, properties, and applications of magnetic iron oxide nanoparticles. jJ. Pcrysgrow. *55*, 22–45.

3. West, A.R. (1999). Basic solid state chemistry (John Wiley & Sons Incorporated).

4. O'Neill, H.S.C., and Navrotsky, A. (1983). Simple spinels; crystallographic parameters, cation radii, lattice energies, and cation distribution. Am. Mineral. *68*, 181–194.

5. Ndione, P.F., Shi, Y., Stevanovic, V., Lany, S., Zakutayev, A., Parilla, P.A., Perkins, J.D., Berry, J.J., Ginley, D.S., and Toney, M.F. (2014). Control of the electrical properties in spinel oxides by manipulating the cation disorder. Adv. Funct. Mater. *24*, 610–618.

6. Kouotou, P.M., Vieker, H., Tian, Z.Y., Ngamou, P.H.T., El Kasmi, A., Beyer, A., Gölzhäuser, A., and Kohse-Höinghaus, K. (2014). Structure–activity relation of spinel-type Co–Fe oxides for low-temperature CO oxidation. Catal. Sci. Technol. *4*, 3359–3367.

7. Goya, G.F., and Rechenberg, H.R. (1999). Ionic disorder and Néel temperature in $ZnFe_2O_4$ nanoparticles. J. Magn. Magn. Mater. *196–197*, 191–192.

8. Zhu, X., Guijarro, N., Liu, Y., Schouwink, P., Wells, R.A., Le Formal, F., Sun, S., Gao, C., and Sivula, K. (2018). Spinel structural disorder influences solar-water-splitting performance of $ZnFe_2O_4$ nanorod photoanodes. Adv. Mater. *30*, 1801612.

9. Marquardt, M.A., Ashmore, N.A., and Cann, D.P. (2006). Crystal chemistry and electrical properties of the delafossite structure. Thin Solid Films *496*, 146–156.

10. Putzke, C., Bachmann, M.D., McGuinness, P., Zhakina, E., Sunko, V., Konczykowski, M., Oka, T., Moessner, R., Stern, A., König, M., et al. (2020). *h/e* oscillations in interlayer transport of delafossites. Science *368*, 1234–1238.

11. Liu, Q.-L., Zhao, Z.-Y., and Yi, J.-H. (2020). Excess Oxygen in Delafossite $CuFeO_{2+\delta}$: Synthesis, Characterization, and Applications in Solar Energy Conversion. Chem. Eng. J. *396*, 125290.

12. Koumoto, K., Koduka, H., and Seo, W.-S. (2001). Thermoelectric properties of single crystal $CuAlO_2$ with a layered structure. J. Mater. Chem. *11*, 251–252.

13. Zhang, H., Wang, H., Chen, W., and Jen, A.K.Y. (2017). $CuGaO_2$: A promising inorganic hole-transporting material for highly efficient and stable perovskite solar cells. Adv. Mater. *29*, 1604984.

14. Nagarajan, R., Duan, N., Jayaraj, M.K., Li, J., Vanaja, K.A., Yokochi, A., Draeseke, A., Tate, J., and Sleight, A.W. (2001). p-Type conductivity in the delafossite structure. Int. J. Inorg. Mater. *3*, 265–270.

15. Shannon, R.D., Rogers, D.B., and Prewitt, C.T. (1971). Chemistry of noble metal oxides. I. Syntheses and properties of ABO_2 delafossite compounds. Inorg. Chem. *10*, 713–718.

16. Jang, Y.J., and Lee, J.S. (2019). Photoelectrochemical Water Splitting with p-Type Metal Oxide Semiconductor Photocathodes. ChemSusChem *12*, 1835–1845.

17. Sivula, K., and Van De Krol, R. (2016). Semiconducting materials for photoelectrochemical energy conversion. Nat. Rev. Mater. *1*, 15010.

18. Prévot, M.S., Guijarro, N., and Sivula, K. (2015). Enhancing the Performance of a robust sol-gel-processed p-type delafossite $CuFeO_2$ photocathode for solar water reduction. ChemSusChem *8*, 1359–1367.

19. Gu, J., Wuttig, A., Krizan, J.W., Hu, Y., Detweiler, Z.M., Cava, R.J., and Bocarsly, A.B. (2013). Mg-doped $CuFeO_2$ photocathodes for photoelectrochemical reduction of carbon dioxide. J. Phys. Chem. C *117*, 12415–12422.

20. Tong, B., Deng, Z., Xu, B., Meng, G., Shao, J., Liu, H., Dai, T., Shan, X., Dong, W., Wang, S., et al. (2018). Oxygen vacancy defects boosted high performance p-type delafossite $CuCrO_2$ gas sensors. ACS Appl. Mater. Interfaces *10*, 34727–34734.

21. Crespo, C.T. (2018). Potentiality of $CuFeO_2$-delafossite as a solar energy converter. Sol. Energy *163*, 162–166.

22. Clause, O., Rebours, B., Merlen, E., Trifiro, F., and Vaccari, A. (1992). Preparation and characterization of nickel-aluminum mixed oxides obtained by thermal decomposition of hydrotalcite-type precursors. J. Catal. *133*, 231–246.

23. Li, M., Yin, Y.-X., Li, C., Zhang, F., Wan, L.-J., Xu, S., and Evans, D.G. (2012). Well-dispersed bi-component-active $CoO/CoFe_2O_4$ nanocomposites with tunable performances as anode materials for lithium-ion batteries. Chem. Commun. (Camb.) *48*, 410–412.

24. Cho, S., Jang, J.W., Kong, K.j., Kim, E.S., Lee, K.H., and Lee, J.S. (2013). Anion-doped mixed metal oxide nanostructures derived from layered double hydroxide as visible light photocatalysts. Adv. Funct. Mater. *23*, 2348–2356.

25. Li, C., Wei, M., Evans, D.G., and Duan, X. (2014). Layered double hydroxide-based nanomaterials as highly efficient catalysts and adsorbents. Small *10*, 4469–4486.

26. Fu, J., DeSantis, C.J., Weiner, R.G., and Skrabalak, S.E. (2015). Aerosol-assisted synthesis of shape-controlled $CoFe_2O_4$: Topotactic versus direct melt crystallization. Chem. Mater. *27*, 1863–1868.

27. Rives, V. (2001). Layered double hydroxides: present and future (Nova Publishers).

28. Sideris, P.J., Nielsen, U.G., Gan, Z., and Grey, C.P. (2008). Mg/Al ordering in layered double hydroxides revealed by multinuclear NMR spectroscopy. Science *321*, 113–117.

29. Bellotto, M., Rebours, B., Clause, O., Lynch, J., Bazin, D., and Elkaïm, E. (1996). A reexamination of hydrotalcite crystal chemistry. J. Phys. Chem. *100*, 8527–8534.

30. Kobayashi, Y., Ke, X., Hata, H., Schiffer, P., and Mallouk, T.E. (2008). Soft chemical conversion of layered double hydroxides to superparamagnetic spinel platelets. Chem. Mater. *20*, 2374–2381.

31. Jeong, I.R., Lee, J.H., Song, J., Oh, Y.S., and Cho, S. (2020). Control of structural disorder in spinel ceramics derived from layered double hydroxides. Ceram. Int. *46*, 6594–6599.

32. Yoon, B., Häkkinen, H., Landman, U., Wörz, A.S., Antonietti, J.-M., Abbet, S., Judai, K., and Heiz, U. (2005). Charging effects on bonding and catalyzed oxidation of CO on Au_8 clusters on MgO. Science *307*, 403–407.

33. Beniya, A., and Higashi, S. (2019). Towards dense single-atom catalysts for future automotive applications. Nat. Catal. *2*, 590–602.

34. Beniya, A., Higashi, S., Ohba, N., Jinnouchi, R., Hirata, H., and Watanabe, Y. (2020). CO oxidation activity of non-reducible oxide-supported mass-selected few-atom Pt single-clusters. Nat. Commun. *11*, 1888.

35. Kang, M.Y., Yun, H.J., Yu, S., Kim, W., Kim, N.D., and Yi, J. (2013). Effect of TiO_2 crystalline phase on CO oxidation over CuO catalysts supported on TiO_2. J. Mol. Catal. Chem. *368–369*, 72–77.

36. Amrute, A.P., Łodziana, Z., Mondelli, C., Krumeich, F., and Perez-Ramirez, J. (2013). Solid-state chemistry of cuprous delafossites: Synthesis and stability aspects. Chem. Mater. *25*, 4423–4435.

37. Musumeci, A.W., Schiller, T.L., Xu, Z.P., Minchin, R.F., Martin, D.J., and Smith, S.V. (2010). Synthesis and characterization of dual radiolabeled layered double hydroxide nanoparticles for use in in vitro and in vivo nanotoxicology studies. J. Phys. Chem. C *114*, 734–740.

38. Parello, M.L., Rojas, R., and Giacomelli, C.E. (2010). Dissolution kinetics and mechanism of Mg-Al layered double hydroxides: a simple approach to describe drug release in acid media. J. Colloid Interface Sci. *351*, 134–139.

39. Rodríguez-Clemente, R., Serna, C.J., Ocaña, M., and Matijević, E. (1994). The relationship of particle morphology and structure of basic copper (II) compounds obtained by homogeneous precipitation. J. Cryst. Growth *143*, 277–286.

40. Smith, R.M., and Martell, A.E. (1976). Critical stability constants: inorganic complexes (Springer).

41. Haraketi, M., Hosni, K., and Srasra, E. (2017). Intercalation behavior of salicylic acid into calcined Cu-Al-layered double hydroxides for a controlled release formulation. Surg. Eng. Appl. Electrochem. *53*, 360–370.

42. Zhao, Y., Zhao, J., Li, Y., Ma, D., Hou, S., Li, L., Hao, X., and Wang, Z. (2011). Room temperature synthesis of 2D CuO nanoleaves in aqueous solution. Nanotechnology *22*, 115604.

43. Jiang, Y., Wu, Y., Xie, B., Xie, Y., and Qian, Y. (2002). Moderate temperature synthesis of nanocrystalline Co_3O_4 via gel hydrothermal oxidation. Mater. Chem. Phys. *74*, 234–237.

44. Zhao, Y., Li, F., Zhang, R., Evans, D.G., and Duan, X. (2002). Preparation of layered double-hydroxide nanomaterials with a uniform crystallite size using a new method involving separate nucleation and aging steps. Chem. Mater. *14*, 4286–4291.

45. Bera, P., Rajamathi, M., Hegde, M.S., and Kamath, P.V. (2000). Thermal behaviour of hydroxides, hydroxysalts and hydrotalcites. Bull. Mater. Sci. *23*, 141–145.

46. Cudennec, Y., and Lecerf, A. (2003). The transformation of $Cu(OH)_2$ into CuO, revisited. Solid State Sci. *5*, 1471–1474.

47. Jenkins, H.D.B., Roobottom, H.K., Passmore, J., and Glasser, L. (1999). Relationships among ionic lattice energies, molecular (formula unit) volumes, and thermochemical radii. Inorg. Chem. *38*, 3609–3620.

48. Hu, W., Donat, F., Scott, S.A., and Dennis, J.S. (2016). The interaction between CuO and Al_2O_3 and the reactivity of copper aluminates below 1000° C and their implication on the use of the Cu–Al–O system for oxygen storage and production. RSC Advances *6*, 113016–113024.

49. Stöcker, T., and Moos, R. (2018). Effect of Oxygen Partial Pressure on the Phase Stability of Copper¯Iron Delafossites at Elevated Temperatures. Materials (Basel) *11*, 1888.

50. Cavani, F., Trifiro, F., and Vaccari, A. (1991). Hydrotalcite-type anionic clays: Preparation, properties and applications. Catal. Today *11*, 173–301.

51. Song, J., Leng, M., Fu, X., and Liu, J. (2012). Synthesis and characterization of nanosized zinc aluminate spinel from a novel Zn–Al layered double hydroxide precursor. J. Alloys Compd. *543*, 142–146.

52. Peck, T.C., Reddy, G.K., and Roberts, C.A. (2019). Monolayer supported $CuOx/Co_3O_4$ as an active and selective low temperature NOx decomposition catalyst. Catal. Sci. Technol. *9*, 1132–1140.

53. Jacob, K.T., and Alcock, C.B. (1975). Thermodynamics of $CuAlO_2$ and $CuAl_2O_4$ and phase equilibria in the system Cu_2O-CuO-Al_2O_3. J. Am. Ceram. Soc. *58*, 192–195.

54. Hernández, M.P., Fernández-Bertrán, J.F., Farías, M.H., and Díaz, J.A. (2007). Reaction of imidazole in gas phase at very low pressure with Cu foil and Cu oxides studied by X-ray photoelectron spectroscopy. Surf. Interface Anal. *39*, 434–437.

55. Yin, M., Wu, C.-K., Lou, Y., Burda, C., Koberstein, J.T., Zhu, Y., and O'Brien, S. (2005). Copper oxide nanocrystals. J. Am. Chem. Soc. *127*, 9506–9511.

56. Wang, P., Ng, Y.H., and Amal, R. (2013). Embedment of anodized p-type Cu_2O thin films with CuO nanowires for improvement in photoelectrochemical stability. Nanoscale *5*, 2952–2958.

57. Liu, Y., Gong, Y., Mellott, N.P., Wang, B., Ye, H., and Wu, Y. (2016). Luminescence of delafossite-type $CuAlO_2$ fibers with Eu substitution for Al cations. Sci. Technol. Adv. Mater. *17*, 200–209.

58. Crêpellière, J., Popa, P.L., Bahlawane, N., Leturcq, R., Werner, F., Siebentritt, S., and Lenoble, D. (2016). Transparent conductive $CuCrO_2$ thin films deposited by pulsed injection metal organic chemical vapor deposition: up-scalable process technology for an improved transparency/conductivity trade-off. J. Mater. Chem. C Mater. *4*, 4278–4287.

59. Han, M., Jiang, K., Zhang, J., Yu, W., Li, Y., Hu, Z., and Chu, J. (2012). Structural, electronic band transition and optoelectronic properties of delafossite $CuGa_{1-x}Cr_xO_2$ ($0 \leq x \leq 1$) solid solution films grown by the sol–gel method. J. Mater. Chem. *22*, 18463–18470.

60. Royer, S., and Duprez, D. (2011). Catalytic oxidation of carbon monoxide over transition metal oxides. ChemCatChem *3*, 24–65.

61. Jernigan, G.G., and Somorjai, G.A. (1994). Carbon monoxide oxidation over three different oxidation states of copper: metallic copper, copper (I) oxide, and copper (II) oxide-a surface science and kinetic study. J. Catal. *147*, 567–577.

62. Huang, T.-J., and Tsai, D.-H. (2003). CO oxidation behavior of copper and copper oxides. Catal. Lett. *87*, 173–178.

63. Busca, G., Lorenzelli, V., Ramis, G., and Willey, R.J. (1993). Surface sites on spinel-type and corundum-type metal oxide powders. Langmuir *9*, 1492–1499.

64. Baidya, T., Murayama, T., Nellaiappan, S., Katiyar, N.K., Bera, P., Safonova, O., Lin, M., Priolkar, K.R., Kundu, S., and Srinivasa Rao, B. (2019). Ultralow-temperature CO oxidation activity of octahedral site cobalt species in Co_3O_4 based catalysts: Unravelling the origin of the unique catalytic property. J. Phys. Chem. C *123*, 19557–19571.

65. Severino, F., Brito, J.L., Laine, J., Fierro, J.L.G., and Agudo, A.L. (1998). Nature of copper active sites in the carbon monoxide oxidation on $CuAl_2O_4$ and $CuCr_2O_4$ Spinel type catalysts. J. Catal. *177*, 82–95.

66. Hornés, A., Bera, P., Cámara, A.L., Gamarra, D., Munuera, G., and Martínez-Arias, A. (2009). CO-TPR-DRIFTS-MS in situ study of $CuO/Ce_{1-x}Tb_xO_{2-y}$ (x= 0, 0.2 and 0.5) catalysts: Support effects on redox properties and CO oxidation catalysis. J. Catal. *268*, 367–375.

67. Gamarra, D., Belver, C., Fernandez-García, M., and Martínez-Arias, A. (2007). Selective CO oxidation in excess H_2 over copper-ceria catalysts: identification of active entities/species. J. Am. Chem. Soc. *129*, 12064–12065.

68. Gamarra, D., Munuera, G., Hungría, A., Fernández-García, M., Conesa, J., Midgley, P., Wang, X., Hanson, J., Rodríguez, J., and Martínez-Arias, A. (2007). Structure–activity relationship in nanostructured copper–ceria-based preferential CO oxidation catalysts. J. Phys. Chem. C *111*, 11026–11038.

69. Liu, Y., Qing, S., Hou, X., Qin, F., Wang, X., Gao, Z., and Xiang, H. (2017). Temperature dependence of Cu–Al spinel formation and its catalytic performance in methanol steam reforming. Catal. Sci. Technol. *7*, 5069–5078.

70. Qi, C., Zheng, Y., Lin, H., Su, H., Sun, X., and Sun, L. (2019). CO oxidation over gold catalysts supported on CuO/Cu2O both in O_2-rich and H_2-rich streams: Necessity of copper oxide. Appl. Catal. B *253*, 160–169.

71. Li, X., Zhang, Q., Xie, H., Gao, X., Wu, Y., Yang, G., Wang, P., Tian, S., and Tan, Y. (2017). Facile Preparation of Cu-Al Oxide Catalysts and Their Application in the Direct Synthesis of Ethanol from Syngas. ChemistrySelect *2*, 10365–10370.

72. Kim, J.Y., Rodriguez, J.A., Hanson, J.C., Frenkel, A.I., and Lee, P.L. (2003). Reduction of CuO and Cu_2O with H_2: H embedding and kinetic effects in the formation of suboxides. J. Am. Chem. Soc. *125*, 10684–10692.

73. Misono, M. (2013). Catalysis of perovskite and related mixed oxides. In In Studies in surface science and catalysis,, M. Misono, ed. (Elsevier), pp. 67–95.

74. Jones, J., Xiong, H., DeLaRiva, A.T., Peterson, E.J., Pham, H., Challa, S.R., Qi, G., Oh, S., Wiebenga, M.H., Pereira Hernández, X.I., et al. (2016). Thermally stable single-atom platinum-on-ceria catalysts via atom trapping. Science *353*, 150–154.

75. Nie, L., Mei, D., Xiong, H., Peng, B., Ren, Z., Hernandez, X.I.P., DeLaRiva, A., Wang, M., Engelhard, M.H., Kovarik, L., et al. (2017). Activation of surface lattice oxygen in single-atom Pt/CeO_2 for low-temperature CO oxidation. Science *358*, 1419–1423.

76. Fan, S., Li, X., Yin, Z., Qin, M., Wang, L., Gan, G., Wang, X., Xu, F., Tadé, M.O., and Liu, S. (2021). Rational design of cobaltate $MCo_2O_{4-\delta}$ hierarchical nanomicrostructures with bunch of oxygen vacancies toward highly efficient photocatalytic fixing of carbon dioxide. J. Phys. Chem. C *125*, 9782–9794.

77. Dey, S., and Dhal, G.C. (2020). Ceria doped CuMnOx as carbon monoxide oxidation catalysts: Synthesis and their characterization. Surf. Interfaces *18*, 100456.

78. Dey, S., and Mehta, N. (2020). Selection of Manganese oxide catalysts for catalytic oxidation of Carbon monoxide at ambient conditions. . Resources, Environment and Sustainability *1*, 100003.

79. Dey, S., and Mehta, N. (2021). To optimized various parameters of Hopcalite catalysts in the synthetic processes for low temperature CO oxidation. Appl. Energy Combust. Sci. *6*, 100031.